A Tejútrendszer kutatása

Puha Emil

Division of Astronomy and Astrophysics, Department of Astronomy, Physics of the Earth and Meteorology,
Faculty of Mathematics, Physics and Informatics, Comenius University in Bratislava

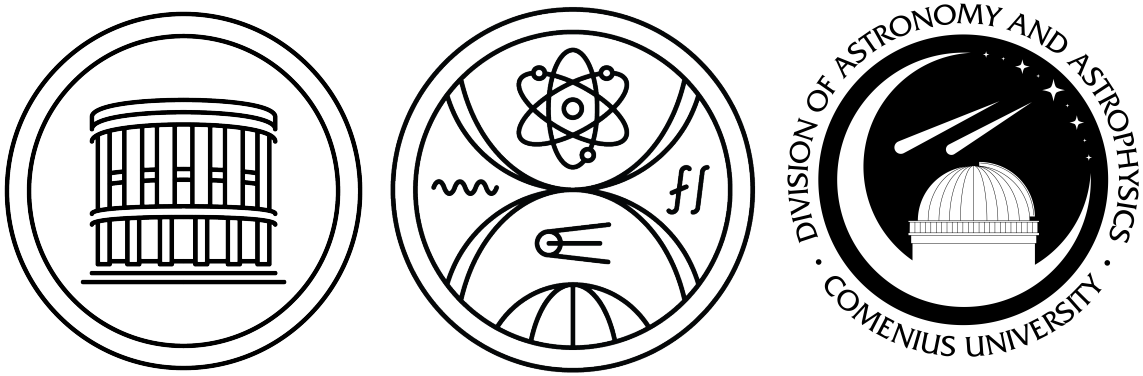

2021.08.09.

Outline

Remnants of a past merger

Helmi et al. (2019)

Evidence for a past merger event (Gaia-Enceladus), which led to the formation of the Milky Way's inner stellar halo and the thick disk.

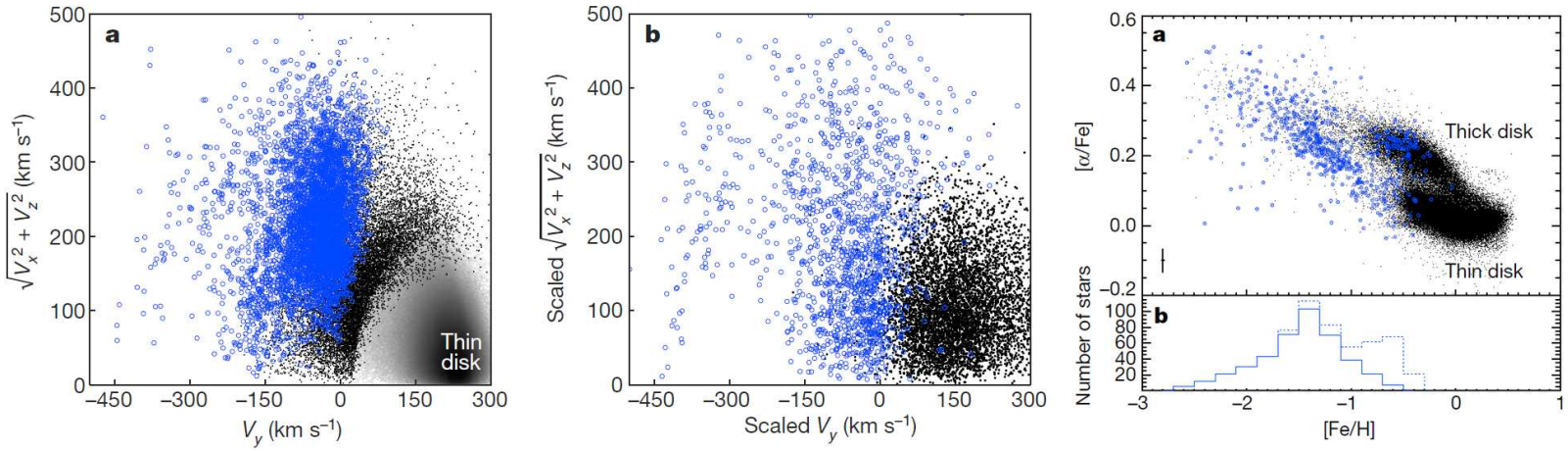

Figure: Left: measured velocity distributions of stars (a) compared with the merger simulation results (b). Disk stars plotted with black colour. Right: chemical abundances of the selected dataset. Blue point are part of a prominent structure with slightly retrograde mean rotational motion.

Dustmap of the Galaxy

Anders et al. (2019)

All-sky median extinction map using the stars up to G < 18 mag from the cross-matched dataset of Gaia, WISE, 2MASS and Pan-STARRS

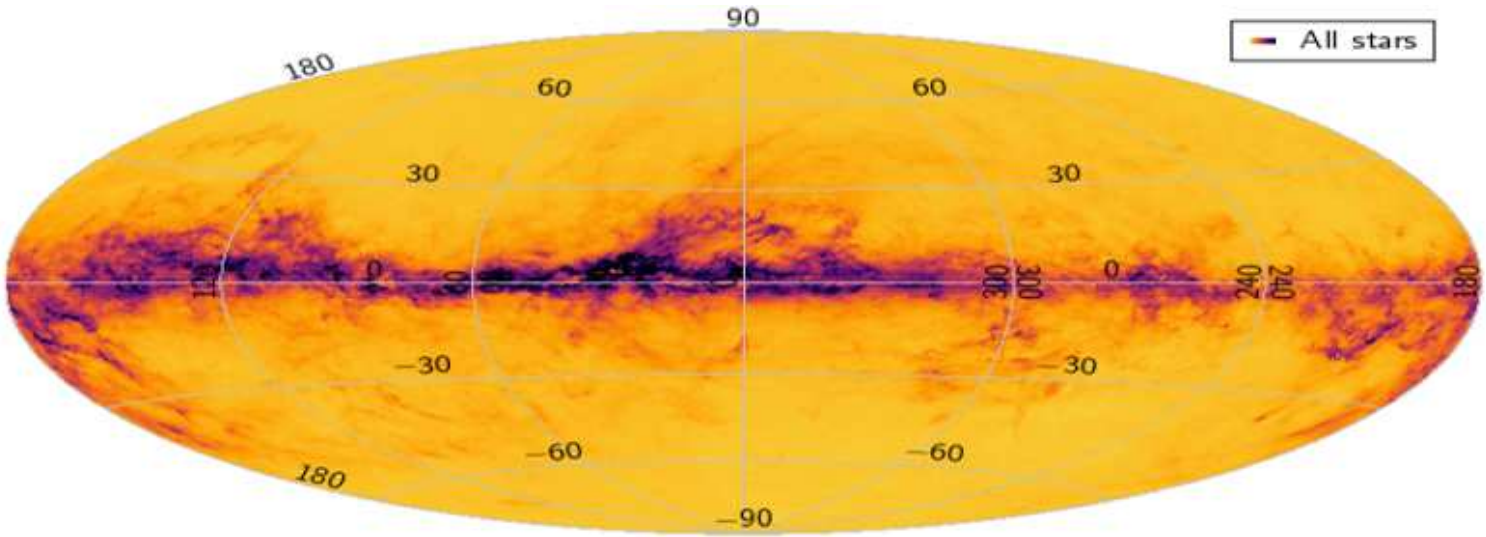

Figure: All-sky median extinction map.

Imaging the Galactic bar

Anders et al. (2019)

First clear manifestation of the Galactic bar in the stellar density distribution

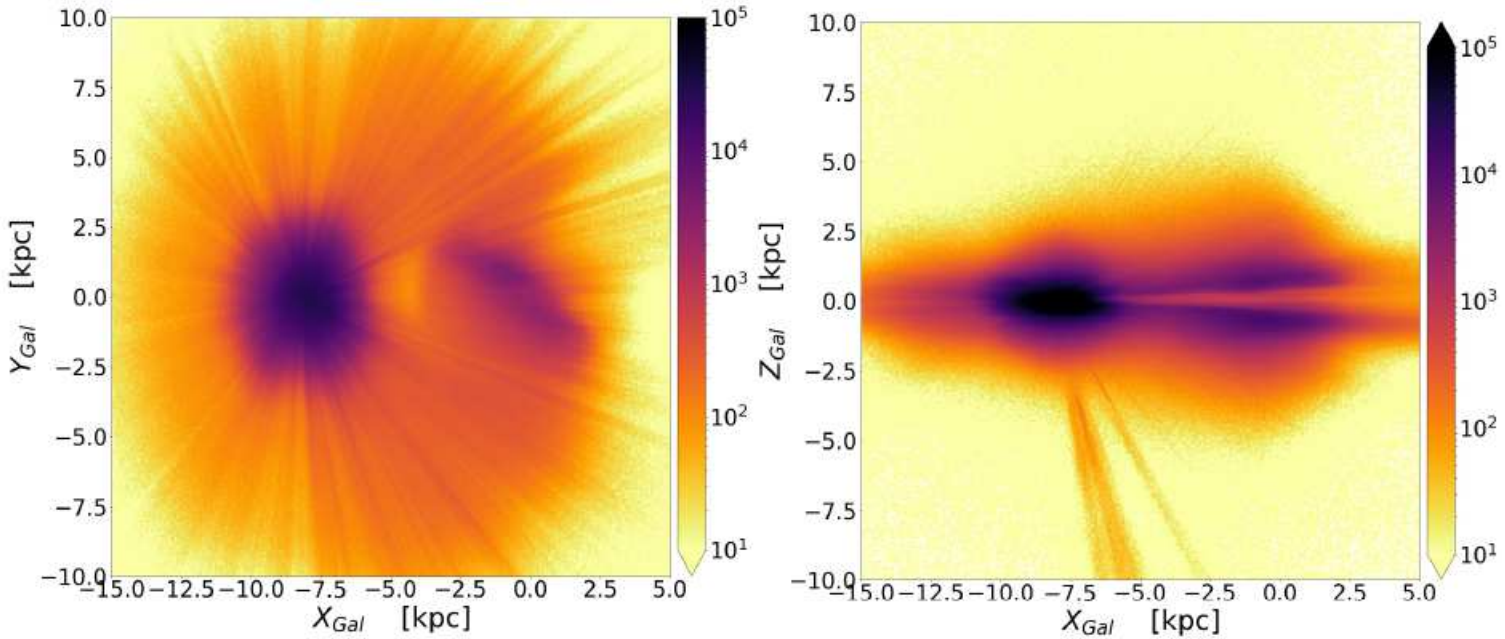

New stellar populations

Carollo et al. (2019)

Thick disk actually consists of two distinct and overlapping stellar populations with different kinematic properties and abundances. Discovery of the metal-weak thick disk (MWTD)

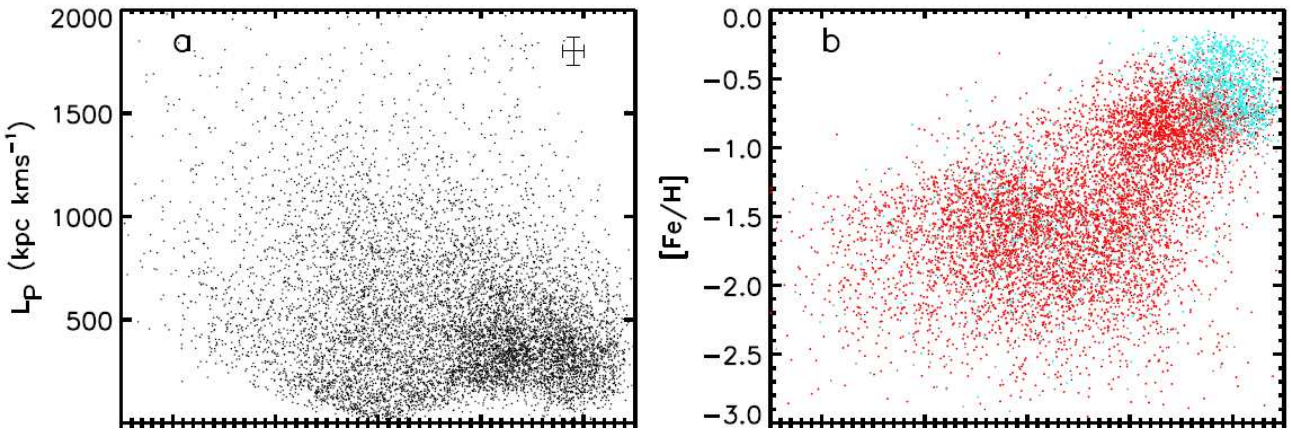

Figure: The Galactic thick disk and it's two components: thick disk (red) and MWTD (cyan). Panel (a) shows the distribution in the L_Z, L_p plane, (b) shows the $L_Z, [Fe/H]$ plane.

Velocity dispersion maps

Katz et al. (2018)

Revealed the complexity of the velocity field in the Galactic disk. A clue, that the Galaxy is not in an axisymmetric equilibrium

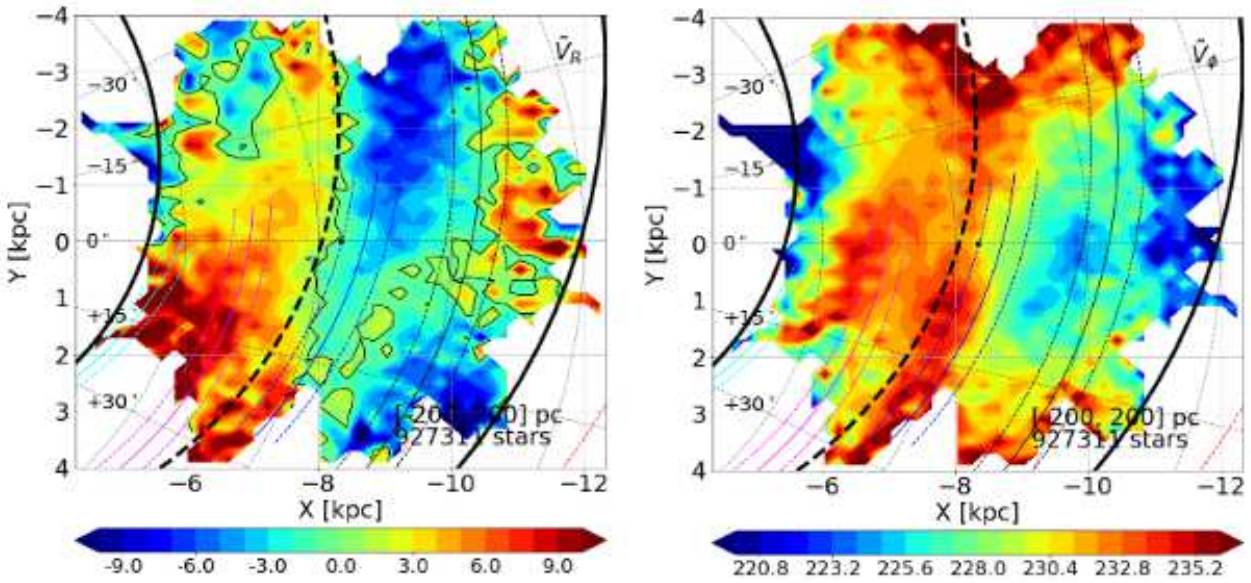

Figure: Left: median radial velocity distribution, right: the median azimutal velocity distribution. The two-arm spiral model over-plotted with black lines.

Imaging the warp & flare

Chrobáková et al. (2020)

Stellar density maps show the presence of a distinct Galactic warp and flare. Support of the theory of warp formation through accretion of stars to the disk

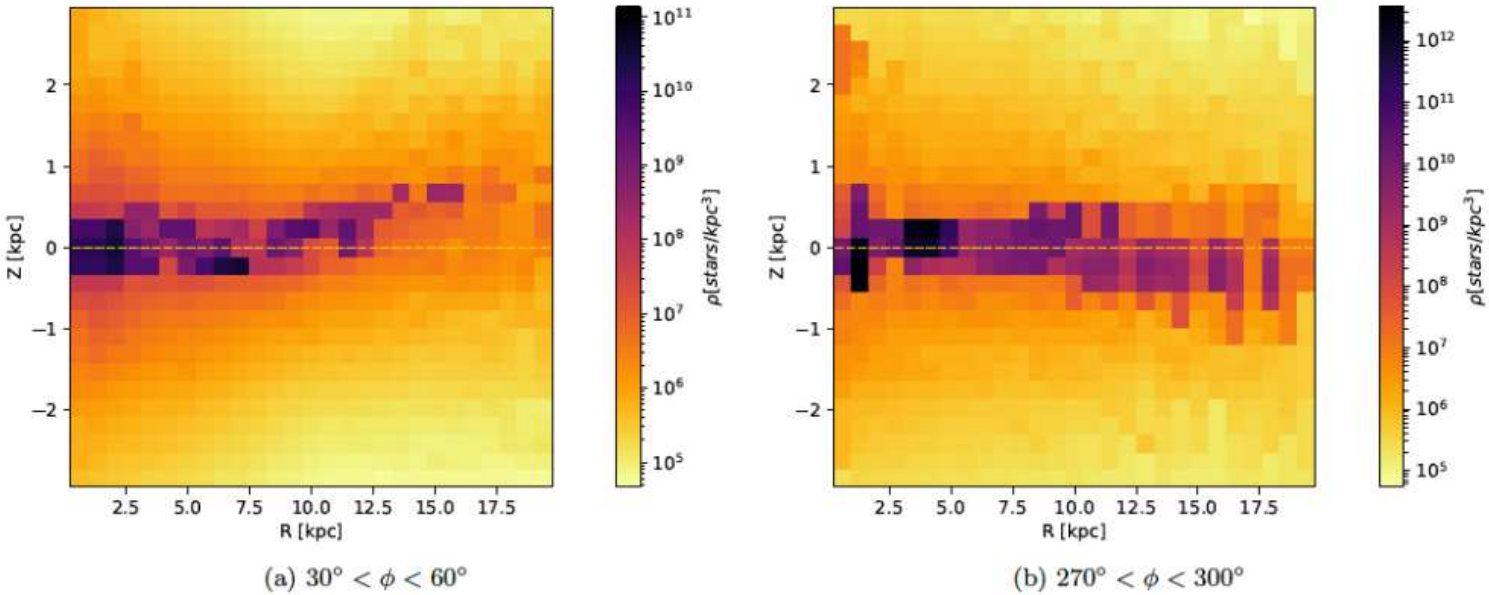

Figure: Density maps showing the warp for various azimuths.

The precessing warp

Poggio et al. (2020)

The warp of the Milky Way galaxy has a precession, which is a result of a recent or ongoing encounter with a satellite galaxy.

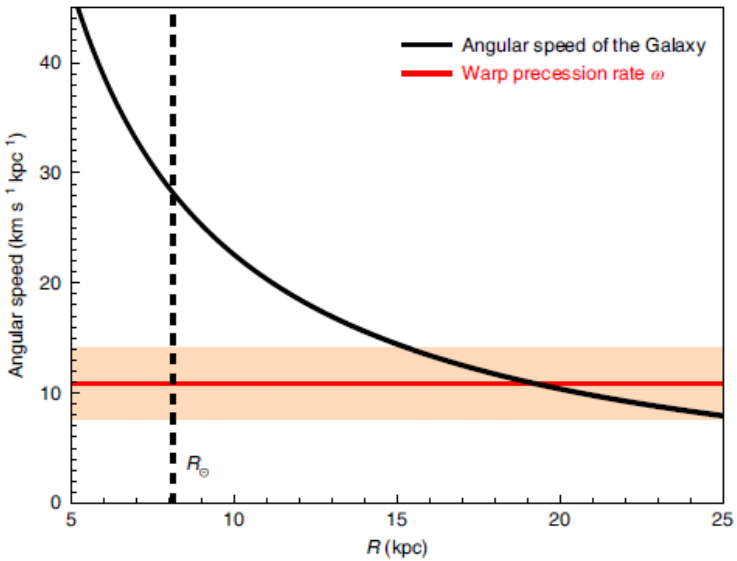

Figure: Comparison of the warp precession rate and the angular speed in the Galaxy. Orange area shows the uncertainty in ω.

The billion star surveyor

Gaia

The Global Astrometric Interferometer for Astrophysics was launched in 2013 as a successor of Hipparcos

Definite catalogue of the foreseeable future

Data collected by Gaia throughout its mission will be used to eventually build the most accurate three-dimensional map of the positions, motions, and chemical composition of stars in our Galaxy

Accuracy of the Gaia parallaxes I

Formal uncertainties (random errors)

in Gaia DR's were estimated from the internal consistency of measurements

- these are the published errors in Gaia DR's

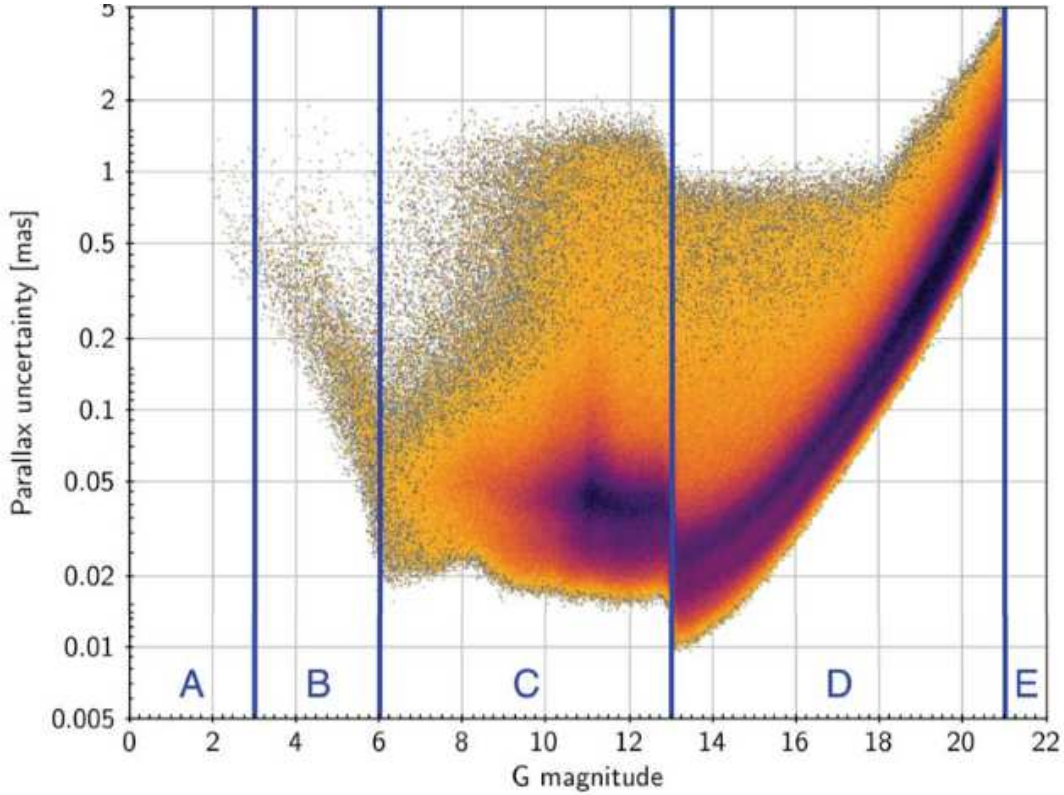

Figure: The cause of errors: (A): too bright, (B): partly saturated (unreliable), (C): detector limitation, (D): limited photon number, (E): too faint (not published). *Credit:* Stefan Jordan

Accuracy of the Gaia parallaxes II

Systematic errors of parallaxes

- depend on position, magnitude, colour, ...
- mean value is the parallax zero-point

Parallax Zero-Point

is the expected measured parallax for a source at infinity

- should be zero for a perfect Gaia with a stable basic angle
- the basic angle varies (amplitude ~ 1 mas)

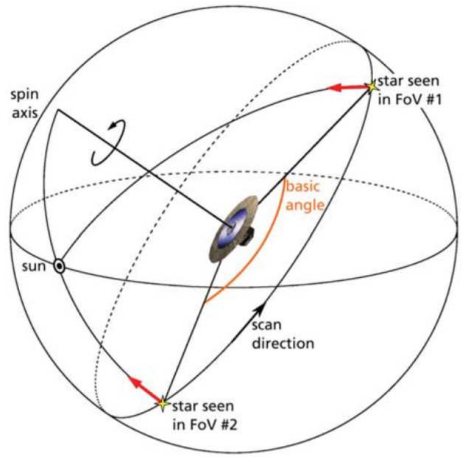

Figure: Basic angle of Gaia. *Credit:* Stefan Jordan

Zero-Point estimation DR2

- Lindegren et al., (2018)
- Zero-point estimated from half a million quasars ("sources in the infinity")

$$-29\ \mu\text{as}$$

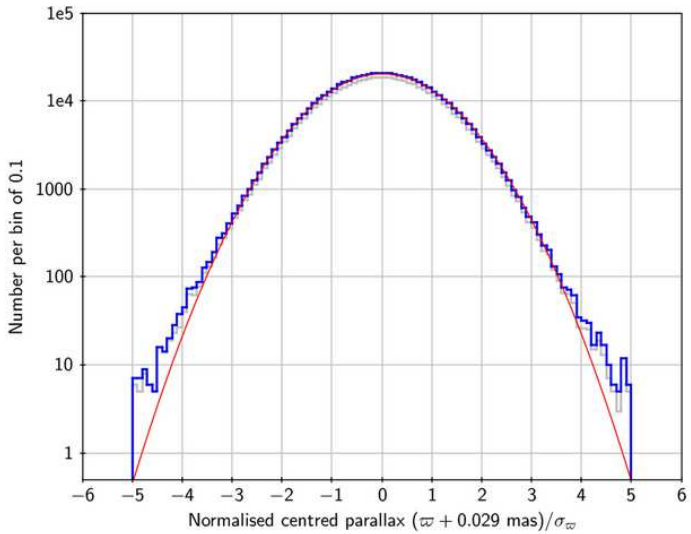

Figure: Distributions of the normalised centred parallaxes. The red curve is a Gaussian distribution with the same standard deviation (1.081) as the normalised centred parallaxes for the full sample. *Credit:* Lindegren et al., (2018).

Zero-Point estimation EDR3

- Lindegren et al., (2020)
- Zero-point estimated from quasars and closer sources
- It varies for different G-band magnitude and color between

$$-94 \text{ to } +35 \ \mu\text{as}$$

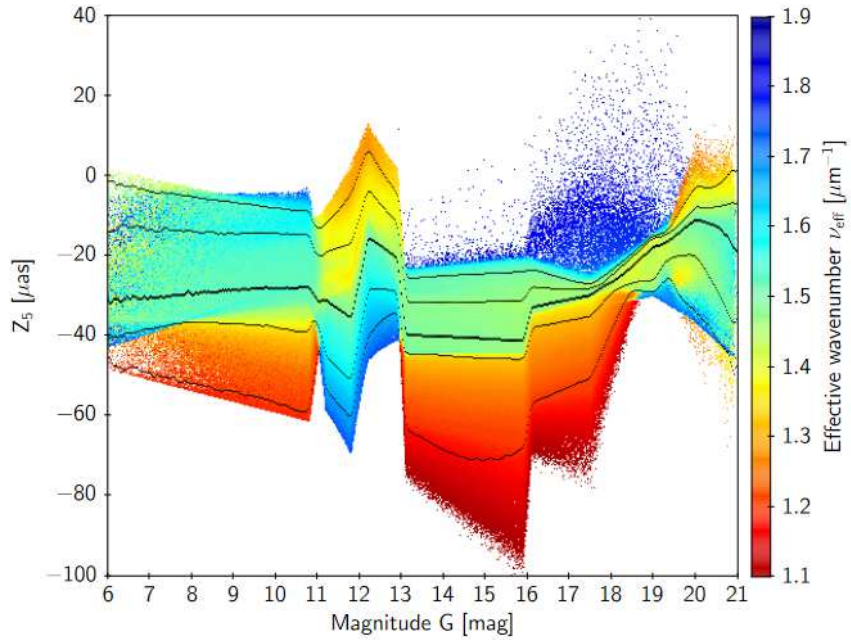

Figure: The parallax bias Z (zero point variation). *Credit:* Lindegren et al., (2020).

Selecting stars with good astrometry

- From Gaia DRs we can obtain unit weight errors (UWE)

$$u = \sqrt{\frac{\text{astrometric\_chi2\_al}}{\text{astrometric\_n\_good\_obs\_al} - 5}}$$

- the weight of the astrometric error along the line of sight
- dividing the UWE with a normalisation function u_0 we obtain the Re-normalised Unit Weight Error (RUWE)

$$\text{RUWE} = \frac{u}{u_0(\text{magnitude, color})}$$

Recommendation for good astrometric solutions

$$\text{RUWE} \leq 1.4$$

$$\text{visibility\_periods\_used} > 8$$

$$1.0 + 0.015(G_{BP} - G_{RP})^2 < \text{flux\_excess\_noise} < 1.3 + 0.06(G_{BP} - G_{RP})^2$$

APOGEE-2

Large-scale survey of Milky Way stellar chemistry and kinematics

Stellar measurements throughout the Galaxy, spanning from the central bulge to the halo

- includes spectra, derived stellar parameters
- abundance measurements of 15 individual elements: C, N, O, Na, Mg, Al, Si, S, K, Ca, Ti, V, Mn, Fe, Ni

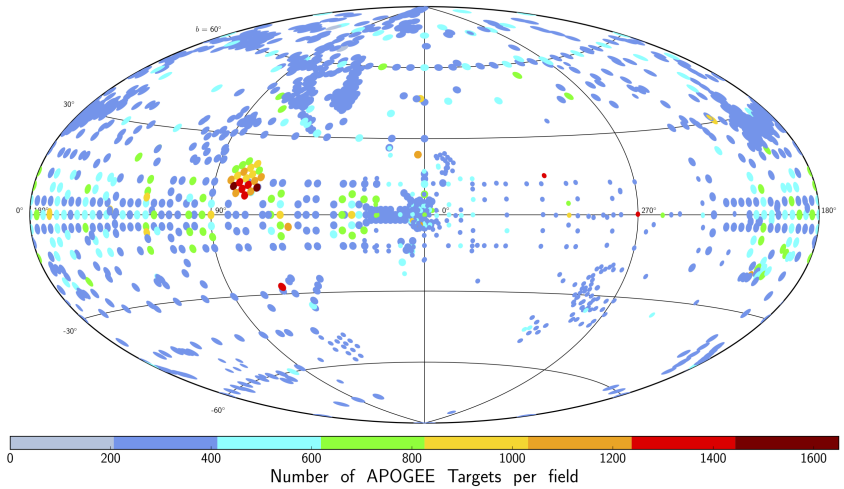

FIGURE: APOGEE observations. *Credit:* SDSS

Data Release 16

Released in 2019

contains new optical and infrared spectra, maps, stellar library spectra and images

- 473 307 observed targets
- stellar spectra
- radial velocities
- stellar parameters - effective temperature, surface gravity, metallicity
- chemical abundances

Gaia and APOGEE

Cross-match of DR16 with Gaia data

provides combination of spectroscopic and astrometric data

- we can determine the spectral types (groups) of APOGEE stars
- we can assign precise astrometric measurements to them via cross-matching with Gaia data

Spectral type (group) determination

Stellar spectral types

could be determined from individual elements abundances, effective temperature ranges and projected rotational velocities

Spectral type (group) determination

Interstellar extinction correction

Interstellar extinction

$$M_G = G - 5\log d + 5 - A_G$$

- Determined magnitudes have to be corrected
- Available packages:
  - `dustmaps` (Green, 2018)
  - `mwdust` (Bovy, 2020)
- Which contain dustmaps from various surveys

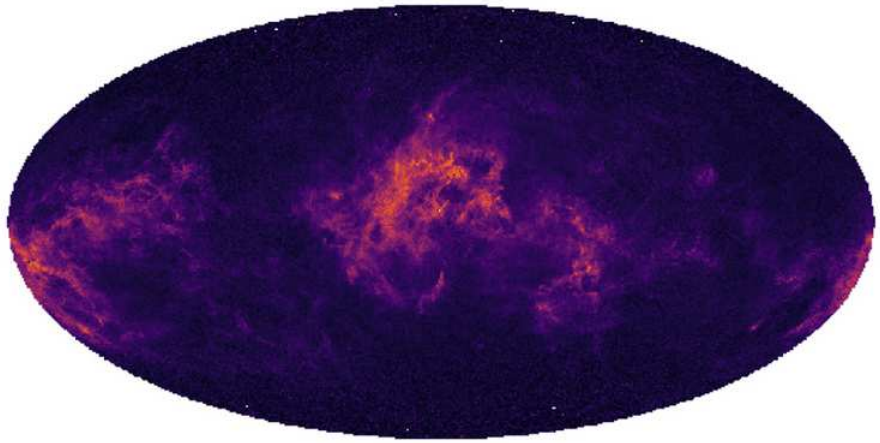

Figure: projection of the G-band extinction. Combined data from surveys such as Gaia, 2MASS, PANSTARRS, and ALLWISE. *Credit:* Leike et al., 2020.

Extinction correction of Gaia data - steps

1. Determine the color excess $E(B-V)$ for every target using dustmaps
2. Determine the line-of-sight extinction in Gaia G magnitude (Chen et al., 2018):
$$A_G = 2.6629\ E(B-V)$$
3. Calculate the absolute magnitude and subtract A_G:
$$M_G = G - 5\log d + 5 - A_G$$
4. $E(B-V)$ can be converted to excess in Gaia colors (Hendy, 2018):
$$E(B-V) = 1.289\ E(G_{BP} - G_{RP})$$

Calculating star counts

To determine stellar density

we need the star count as a function of distance

- Parallax error increases with distance (accurate data up to 5 kpc)
- Accurate distance measurement up to 20 kpc could be obtained via Lucy's deconvolution method (López-Corredira & Sylos-Labini, 2019; Lucy, 1974)
- Observed number of stars per parallax $\overline{N}(\pi)$ is a convolution of the real number $N(\pi)$ and a Gaussian:

$$\overline{N}(\pi) = \int_0^\infty \mathrm{d}\pi' \; N(\pi') G(\pi - \pi')$$

- Where σ_π of the Gaussian is the averaged error for every data bin

Lucy's method (for the inversion of Fredholm integral equations of the first kind)

- The function $N(\pi)$ is determined via iterative Lucy's method:

$$N(\pi) = \lim_{n\to\infty} N_n(\pi)$$

$$N_{n+1}(\pi) = N_n(\pi)\frac{\int_0^\infty \frac{\overline{N}(\pi')}{\overline{N}_n(\pi')} G_{\pi'}(\pi-\pi')\ \mathrm{d}\pi'}{\int_0^\infty G_{\pi'}(\pi-\pi')\ \mathrm{d}\pi'}$$

$$\overline{N}_n(\pi) = \int_0^\infty N_n(\pi')G_{\pi'}(\pi-\pi')\ \mathrm{d}\pi'$$

- The iteration converges when:

$$\overline{N}_n(\pi) \sim \overline{N}(\pi)\forall\pi$$

Age determination from kinematical data

Almeida-Fernandes & Rocha-Pinto, (2018)

developed a method to determine stellar ages from peculiar velocities U, V and W and their eccentricities

- Velocity dispersion of a stellar group is larger, the older is the group (Rocha-Pinto, 2004)
- Result of gravitational perturbations experienced by the stars during their translations around the galactic center
- The Age-velocity dispersion relations can be approximated by power laws of kind

$$\sigma \propto \left(1 + \frac{t}{\tau}\right)^{\chi}$$

where τ is the time scale of growth and t is the stellar age

Age determination from kinematical data

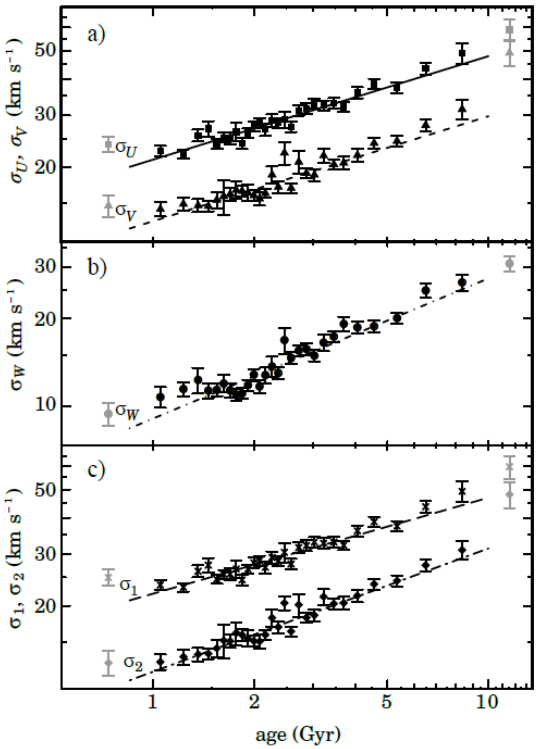

Figure: Velocity dispersion as a function of age for the U (squares, solid line), V (triangles, dashed line) and W (circles, dot dashed line) components. *Credit:* Almeida-Fernandes & Rocha-Pinto, (2018)

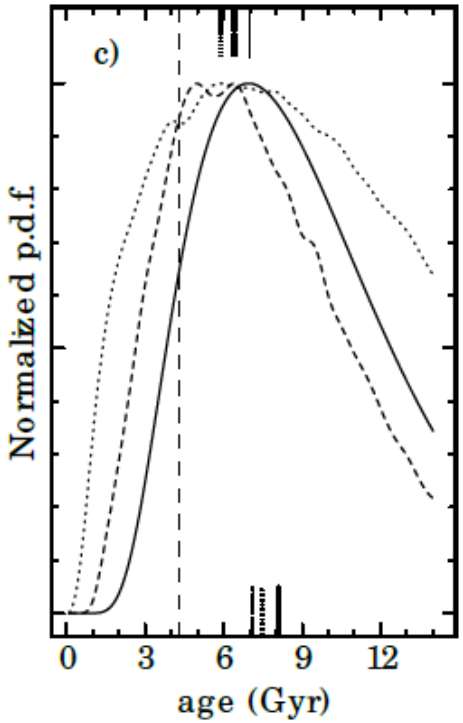

Figure: Probability density function obtained by Method UVW (solid line), Method eVW (dashed line) and Method eUW (dotted line), for four representative stars.The vertical marks at the top axis represents the most likely age for each method and those at bottom axis represents the expected ages. *Credit:* Almeida-Fernandes & Rocha-Pinto, (2018)

Stellar luminosity functions I

Stellar LF's

are basic statistical descriptors of stellar populations: probability distribution for stellar luminosities and masses

- Measures number of stars in an absolute magnitude interval $M + \mathrm{d}M$ in a volume element $\mathrm{d}V$

$$\Phi(M) = \frac{\mathrm{d}N}{\mathrm{d}M}$$

- Seeliger (1898) the estimate of $\Phi(M)$ is essential in determining the structure of the Galaxy, as the observed number-magnitude distribution of stars $A(m)$ could be expressed as

$$A(m) = \omega \int \Phi(M - a(r))\ D(r)\ r^2\ \mathrm{d}r,$$

where $a(r)$ is the extinction, $D(r)$ is a volume element and ω is the angle covered by the observations

Stellar luminosity functions II

Initial Mass Functions

are derived from stellar LF's

- The number of stars that have been born with initial masses between $M + \mathrm{d}M$ (here M is for masses)

$$\xi(M) = \frac{\mathrm{d}N}{\mathrm{d}M}$$

- Both stellar luminosities and masses are connected via the mass-luminosity relation

$$\frac{L}{L_\odot} = \left(\frac{M}{M_\odot}\right)^\alpha$$

LF determination from Gaia data

- One can determine LF's from Gaia data with the use of the V_{max} technique (Schmidt, 1968) . (maximum volume probed at a given absolute magnitude, corrected to take the decrease in stellar density with increasing distance above the Galactic plane):

$$V_{max} = \Omega \frac{H^3}{\sin^3 b} [2 - (\xi^2 + 2\xi + 2) \exp(-\xi)]$$

$$\xi = \frac{d_{max} \sin b}{H}$$

where H i disk scale height, d_{max} - max. distance of detection, b - latitude, Ω - HEALpix area and H is kind of a constant

LF determination from Gaia data

- d_{max} should be estimated for each object. Thus the object has to be counted as the inverse of the maximum volume V_{max} in which it is observed
- The luminosity function is the sum over all objects within an absolute magnitude bin

$$\Phi(M) = \sum \frac{1}{V_{max}}$$

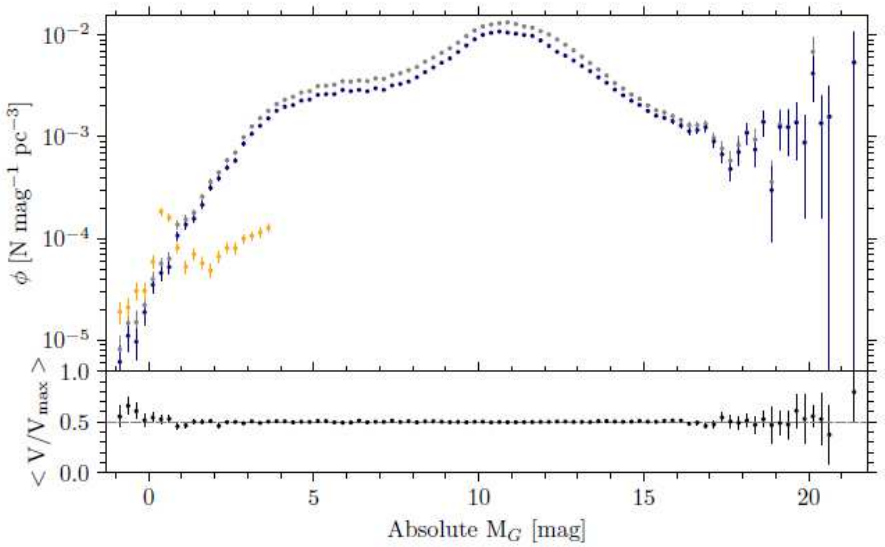

FIGURE: Luminosity function with a 0.25 bin. The upper full curve plotted in grey shows main sequence stars. Full curve plotted in blue is probably for single stars. The small lower partially orange curve shows giants stars. *Credit:* Gaia Collaboration, (2020)

Thank you for your attention